Electronic states of Ag thin films with a laterally periodic insertion of stacking faults

Katsuyoshi Kobayashi
Department of Physics, Faculty of Science, Ochanomizu University, 2-1-1 Otsuka, Bunkyo-ku, Tokyo 112-8610, Japan

Takashi Uchihashi
National Institute for Materials Science, 1-1 Namiki, Tsukuba, Ibaraki 305-0044, Japan

(Received 1 December 2009; published 7 April 2010)

Electronic states of Ag thin films containing stacking faults periodically in a direction parallel to the surface are studied theoretically. Such Ag stacking-fault superlattice thin films were recently fabricated on the Si(111)4×1-In surface, and the formation mechanism of the one-dimensional electronic states observed in photoemission experiments has not been clarified. These systems are suitable for studying stacking faults on nanometer scales in well-defined conditions. Main results obtained in the present study are threefold. One is that the double stacking-fault model proposed in this paper reproduces better the observed dispersions than the originally proposed model. In addition the fact that the stacking-fault thin films have the (111) surface is the origin of the strong deformation near the bottom of the quantized subbands. Second is that the tilt of the stacking-fault plane with respect to the normal of the surface causes mixing of states in different subbands, which is an important factor to form the flat band structures observed. Third is the discussion on the mechanism of the anomalous perfect transmission through the bulk stacking faults of noble metals. In contrast to usual potential scattering, stacking faults change only the phase of orbitals. The condition for perfect transmission is that the effects of scattering are canceled out by renormalization using single phase factor, which is excellently satisfied in the case of noble metals. In addition the symmetry in atomic positions between regular and stacking-fault structures with respect to an axis is the origin of the directional dependence of transmission property.

DOI: 10.1103/PhysRevB.81.155418 PACS number(s): 73.20.At, 73.21.Cd, 61.72.Nn, 73.61.At

I. INTRODUCTION

The face-centered-cubic (fcc) lattice is a stack of two-dimensional hexagonal layers with a constant translation parallel to the layers at each stacking. A stacking fault is generated by changing the direction of translation at a stacking. Stacking faults are naturally included in bulk crystals and may not be rare structures.[1,2] However, it seems difficult to study the stacking faults made in controlled conditions on nanometer scales. In particular it would be more difficult to study directly the electronic properties of stacking faults. The recent fabrication of Ag thin films grown on Si(111)4×1-In surface[3] provides a system suitable for studying stacking faults on nanometer scales because stacking faults are spontaneously inserted in the Ag thin films with a constant period in order to minimize the lattice mismatch with the substrate. This superlattice structure opens a new possibility of studying the electronic properties of stacking faults in the reciprocal space by experimental methods such as photoemission. This paper presents a theoretical study on the electronic structures of the Ag thin films containing stacking faults periodically.

The Si(111)4×1-In surface has a one-dimensional atomic structure determined by surface x-ray diffraction[4] and first-principles calculations.[5–7] The In atoms adsorbed on the Si(111) surface form pairs of zigzag chains, which are periodically arranged in the direction perpendicular to the chains. The Ag thin films grown on this surface have (111) surfaces, and the lattice constants of the films and substrate are mismatched. As a structure releasing this mismatch, a model with periodic insertion of stacking faults in the films was proposed.[3] In this model stacking faults are inserted every five layers in the direction perpendicular to the In chains. The insertion of stacking faults reduces the lattice mismatch in this direction from 6% to 3.8%.

The energy-band structures of the Ag films on Si(111)4×1-In surfaces were obtained from angle-resolved photoemission spectroscopy, where highly anisotropic band dispersions were observed near the Fermi energy.[8,9] The observed two-dimensional bands are quantized due to the finite-size confinement effect of the thin films in the direction perpendicular to the surfaces. The dispersions parallel to the In chains are like free electrons. This result agrees with the free-electron-like *sp* bands of bulk Ag except for the neck regions. However, the bands perpendicular to the In chains show flat dispersions near the zone center, which indicates that electrons are confined in the direction perpendicular to the In chains as well as the thickness direction of the thin films, and one-dimensional electronic states are formed in the Ag films.

This drastic change in electronic states may be an unexpected result because stacking faults are expected to give only small perturbation to the electronic states in fcc noble metals. The distances and numbers of the first and second nearest-neighbor atoms are unchanged at a stacking fault. The reflection by a stacking fault for the electrons at the Fermi energy is negligibly small in the most region of the Brillouin zone except for the neck parts.[10] It is not obvious why electrons are confined by stacking faults in the Ag films. A purpose of the present paper is to investigate theoretically whether electrons are confined by stacking faults, and to clarify the origin of the one-dimensional electronic states observed in the photoemission experiment. In this paper we propose an atomic structure different from the original one,[3]

and show that the electronic structure of this proposed model better reproduces the photoemission data. We present also a discussion on the origin of the anomalous perfect transmission through the bulk stacking faults of noble metals in terms of a scattering property specific to stacking faults. That is the property that stacking faults change only the phase of orbitals.

There are several theoretical studies on the electronic states of stacking faults and related structures. Stiles and Hamann studied the electron transmission through a Si(111) twin boundary, and found the difference in transmission behavior between split-off hole states and the light-hole and heavy-hole states near their band extrema.[11] They also studied the electron transmission through Si stacking faults as a function of the separation of two twin boundaries forming a stacking fault.[12]

Murayama and Nakayama studied electronic structures of heterocrystalline semiconductor superlattices.[13,14] They found that the quantum-well picture is valid for the states around fundamental band gaps[13] and explained the difference in band offsets between zone centers and zone boundaries by the phase matching of wave functions.[14] Ikonić, Srivastava, and Inkson studied the electronic states of twinning semiconductor superlattices, and found several properties of minibands specific to twinning superlattices.[15,16]

A characteristic difference from the superlattice systems mentioned above is that the Ag thin film superlattices has finite sizes in a direction different from that of the stacking faults. In addition to the formation of superlattices in one dimension by stacking faults, electrons are confined in another dimension by vacuum and substrates.

It seems that the finite-size effect merely results in quantization of states. However, there is a distinct feature in the present system. The stacking-fault plane is not perpendicular to the surface plane. This tilting structure makes electron scattering complex, which gives rise to some effects different from simple quantization on band structures. It will be revealed that the titling effect plays an important role in the formation of the band structures observed in the photoemission experiments.

The method of calculations is presented in Sec. II. Calculated results are shown in Sec. III where transmission properties through a bulk stacking fault, electronic structures of a bulk stacking-fault superlattice, and electronic structures of thin films containing periodically stacking faults are presented. Conclusions are presented in Sec. IV.

II. METHOD OF CALCULATIONS

Though the Ag films used in the experiments[3,8,9] are grown on the Si(111)4×1-In surface, we calculate electronic states of free-standing Ag films in the present study. The main reason for this simplification is to perform calculations within a reasonable computational time. Another reason is that photoemission experiments are sensitive to the states near surfaces. We compare the calculated results mainly with the photoemission data in this paper. The interaction with substrates can cause such effects as charge transfer and bonding between the atoms in Ag films and substrates, and the wave function of the Ag films is expected to be modified. However, the effects of charge transfer and bonding are usually localized within a few atomic distance due to the screening, and the atomic-scale deformation in the wave function also decays with the distance from interfaces.[17] Therefore the wave function near surfaces does not much differ between the free-standing films and the films on substrates for the relatively thick films used in experiments. The interaction with substrates may make the electron confinement in Ag films incomplete and give rise to a change in the phase of reflection. These effects will appear as energy shifts and broadening of quantized levels. However, these effects are not essential problems in the discussion on the formation mechanism of the one-dimensional electronic states. As will be shown in the results, characteristic features observed in the experiments can be reproduced by the present calculation.

Even in the case of free-standing films, we have to calculate electronic structures of the systems that contain typically 100 Ag atoms in a unit cell. The thickness of the Ag films used in the photoemission experiments is 15–30 layers,[8,9] and the stacking faults are inserted every five layers in a direction parallel to the surfaces.[3] Since it is difficult to calculate electronic states of such systems directly by the first-principles methods, we take a two-step approach.

First we calculate the electronic structures of bulk Ag and Ag thin films by a density-functional method. We determine tight-binding parameters to reproduce the band structures obtained by the density-functional calculations. Then we calculate the electronic structures of Ag thin films with stacking faults by a tight-binding method.

A. Density-functional calculation

We use program package PHASE for density-functional calculations.[18] Wave functions are expanded in terms of plane waves. The ultrasoft pseudopotential by Vanderbilt is used for the effective potential of ions.[19] The generalized gradient approximation by Perdew, Burke, and Ernzerhof is used for the exchange-correlation energy.[20] The cutoff energies for expanding wave functions and charge density are 25 and 225 Ry, respectively. We calculate the band structures of bulk Ag in fcc structure and Ag (111) thin films. We use a $8\times8\times8$ uniform mesh for sampling wave vectors in the Brillouin zone of bulk Ag. We use the band structure of a system containing 12 Ag layers and a vacuum region in the unit cell to determine the tight-binding parameters of thin films. The size of the vacuum region is 3 atomic layers. We checked the convergence of band calculations by increasing the size of the vacuum region to 4 atomic layers. The sampling of wave vectors in the calculation of films is a 8×8 mesh in the two-dimensional Brillouin zone parallel to the surface plane, and one point in the perpendicular direction. Atomic positions are not relaxed in the calculation of thin films.

B. Tight-binding calculation

We use a simple tight-binding method. We take account of only the onsite energy and the nearest-neighbor transfer en-

TABLE I. Tight-binding parameters. Energy is shown in eV.

$V_{ss\sigma}$	$V_{sp\sigma}$	$V_{sd\sigma}$	$V_{pp\sigma}$	$V_{pp\pi}$	$V_{pd\sigma}$	$V_{pd\pi}$	$V_{dd\sigma}$	$V_{dd\pi}$	$V_{dd\delta}$
−0.8792	1.1170	−0.4544	1.1892	−0.5933	−0.5310	0.2060	−0.4381	0.2472	−0.0581

ε_s	ε_p	ε_d	$\Delta\varepsilon_s^{SF}$	$\Delta\varepsilon_p^{SF}$
2.8136	6.6392	−4.1813	−1.4603	−1.9012

ergy, and neglect the higher-order transfer energies and overlap integrals. The atomic orbitals used are 6*s*, 6*p*, and 5*d* orbitals.

First we determine the tight-binding parameters to reproduce the band structure of bulk Ag obtained by the density-functional calculation. Second we change the parameters to reproduce the band structure of the Ag thin film with fixing the parameters related to *d* orbitals. The free parameters are those within *s* and *p* orbitals. This two-step fitting is necessary for determining the parameters which reproduce the position of the *sp* surface-state band of the Ag(111) surface as explained below.

In the first step the parameters are determined to fit the lowest six energy levels at Γ and seven levels at *X* and *L* points in the Brillouin zone of the bulk fcc structure. Since the highest level used for fitting is located 6.7 eV above the Fermi energy, the band structure obtained by a tight-binding calculation well reproduces that by the density-functional calculation in the region below this energy level. The differences in energy at the levels used for fitting is less than 0.1 eV except for two levels in *d* bands where the maximum difference is 0.21 eV. However, since this paper deals with the *sp* bands near the Fermi energy, this difference in *d* bands is not a serious matter.

We calculate the energy bands of Ag thin films using the parameters obtained by fitting to the bulk bands, and find two features by comparing the results of the tight-binding and density-functional calculations. One is that *d* bands which are located in the energy range from 3 to 6 eV below the Fermi energy are well reproduced. Second one is that the surface-state band appearing in the *sp*-hybridization gap of bulk bands is higher by about 2 eV in the tight-binding bands than the density-functional one. Since we discuss the electronic states near the Fermi energy in this paper, *d* bands are not so important. Therefore we fix the parameters related to *d* bands. However, the surface-state bands which are located near the Fermi energy in the experiments and the density-functional calculation should be accurately reproduced. Since the wave function of the surface state is mainly composed of *s* and *p* orbitals, the parameters of these orbitals are changed. In the fitting we regard the onsite energies of the outermost and inner layers as independent parameters. This increases the number of fitting parameters, and enables to reduce the deviation of the parameters for inner layers from those fitted to bulk bands.

Table I shows the tight-binding parameters finally determined. ε_i $(i=s,p,d)$ shows onsite energy. V_{ijk} $(i,j=s,p,d;k=\sigma,\pi,\delta)$ shows transfer energy between i and j atomic orbitals in k configuration. $\Delta\varepsilon_s^{SF}$ and $\Delta\varepsilon_p^{SF}$ are differences in onsite energies of the outermost layers from the inner layers. The origin of energy is the Fermi energy.

Figure 1 shows band structures of a Ag(111) film obtained by the density-functional method and a tight-binding calculation using the parameters shown in Table I. The tight-binding parameters are determined to fit the levels between 3.1 and 4.1 eV at the $\bar{K}$ point, between −2.9 and 3.8 eV at the $\bar{\Gamma}$ point, between −0.3 and 3.5 eV at the $\bar{M}$ point, and the lowest level at the $\bar{\Gamma}$ point. As will be shown in the results, the band structure in the range of a few eV around the Fermi energy is important in this paper, which is reasonably reproduced.

The electronic structure given by the present tight-binding parameters reproduces the data experimentally obtained. The neck and belly structure is a characteristic of the bulk Fermi surfaces of noble metals. The radii of the belly and neck are 0.806 and 0.120 in units of $2\pi/a$ estimated from the bands on Γ-*X* and *L*-*W* lines, respectively. a is the loattice constant. The corresponding experimental values are about 0.819 and 0.106.[21]

The band structure of the (111) surface is also reproduced. We calculate the band structure of a Ag(111) film consisting of 50 layers. The energy at the bottom of the *sp* surface-state band is −64 meV, which is close to −63 meV obtained by a photoemission experiment.[22] The effective mass of the surface-state band is $0.395m_e$ and Fermi wave number is 0.081 Å^{-1}, where m_e is the electron mass. The experimental values are $0.397m_e$ and 0.080 Å^{-1}.[22] The binding energy of the bulk state of the (111) surface is 0.49 eV at $\bar{\Gamma}$ point, and the Fermi wavelength is 0.18 Å^{-1}. The experimental values are 0.416 and 0.418 eV, and 0.153 and 0.176 Å^{-1}.[23]

We tried to use the tight-binding parameters including the second nearest-neighbor transfer.[24] However, we do not use

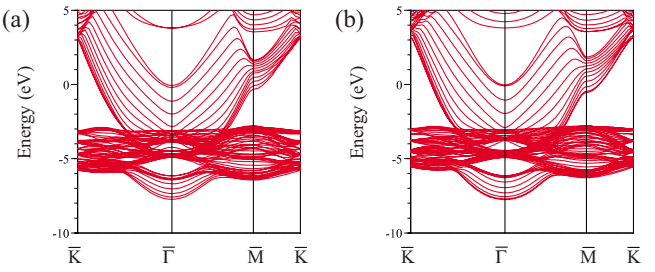

FIG. 1. (Color online) Energy bands of a 12-layer Ag(111) film obtained by a density-functional calculation (a) and a tight-binding calculation (b). The origin of energy is the Fermi energy. The labels for high-symmetry points in the two-dimensional Brillouin zone are defined in Fig. 2.

them because the positions of the *sp* surface-state bands of Ag (111) films calculated using them are too high to reproduce the experimental one. As will be shown in the calculated results, tight-binding calculations using only the present nearest-neighbor transfer parameters essentially reproduce the electronic states of systems including stacking faults.

C. Calculation of transmission

We calculate the transmission properties through a stacking fault using a usual method.[25] First we calculate a transfer matrix of a periodic system in the tight-binding method. All Bloch states including evanescent modes are obtained by diagonalizing the transfer matrix. The wave function of a system containing a scattering structure is expressed in terms of linear combination of an incident wave and reflected waves for the periodic region of the incident side, and transmitted waves for the transmitted side. The Schrödinger equation in the scattering region gives a linear equation for the coefficients of the reflected and transmitted waves and the wave functions in the scattering region. The transmission and reflection coefficients are determined by solving the linear equation.

III. CALCULATED RESULTS

A. Bulk stacking faults

1. Transmission through a stacking fault

Figure 2 shows two-dimensional maps of reflection probability of a stacking fault. The reflection probability is calculated as a function of the two-dimensional wave vector parallel to the stacking-fault plane for fixed energy. Eigenvalues of the transfer matrix are obtained in the calculation of reflection probability. The phase of the eigenvalue for the state with positive group velocity is shown in Fig. 2(c) as a function of the parallel wave vector. Energy is the Fermi energy. The phase is equivalent to the wave number multiplied by the lattice constant in the direction perpendicular to the stacking-fault plane. Therefore this map expresses the constant-energy surface at the Fermi energy in the three-dimensional reciprocal space of bulk Ag viewed from a standpoint in the [111] direction. There is no propagating state in the circle centering the $\bar{\Gamma}$ point and the triangular regions centering the $\bar{K}$ points. The necks of the Fermi surface of bulk Ag are located near the $\bar{M}$ points and the $\bar{\Gamma}$ point.

The reflection probability is zero or nearly zero in the most region. Reflection is finite only near the rims of the constant-energy surfaces. In addition, there is directional dependence. Reflection is almost zero on the $\bar{\Gamma}$-$\bar{K}$ line. These features are the same as those by Bross calculated for Cu.[10] The reflection probability at the $\bar{M}$ point for the Fermi energy is 0.89 in the present calculation and 0.70 by Bross. These results show the similarity of the scattering property of stacking faults in noble metals.

These transmission properties are unusual, and have several points different from the usual transmission. In the usual

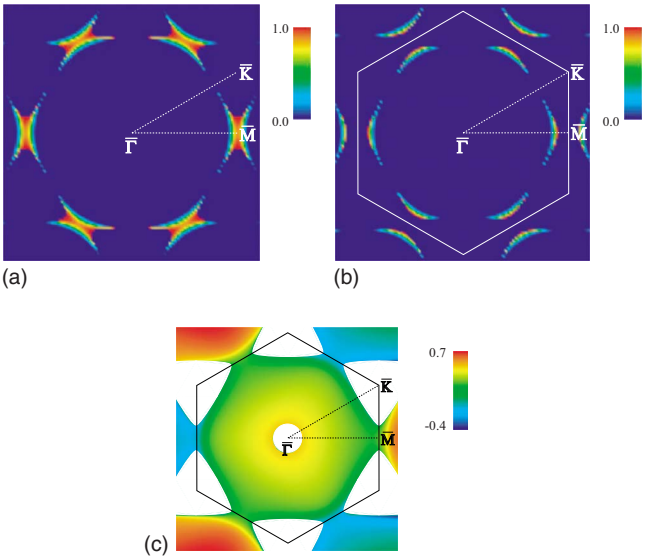

FIG. 2. (Color online) (a) (b) two-dimensional maps of reflection probability of a stacking fault. Energy is the Fermi energy (a) and 1 eV below the Fermi energy (b). The reflection probability is high and low in the red and green regions. That in the blue regions is zero or almost zero. Hexagons show the Brillouin zone. (c) constant-energy surface at the Fermi energy obtained from the phase of eigenvalue of a transfer matrix. The phase is calculated for the state with positive group velocity, and expressed in the units of 2π. There is no propagating state in the white regions.

transmission of a free electron through a potential barrier it is natural that reflection is strong near the rim of a constant-energy surface. This is due to the fact that the longitudinal kinetic energy is smaller than the barrier height near the rim. However the reflection of the stacking fault is zero on the circular rim near the $\bar{\Gamma}$ point. Moreover, the reflection in the usual transmission is finite even in the region apart from the rim, which is in contrast to the almost perfect transmission through the stacking fault. The absence of reflection near the $\bar{\Gamma}$ point may be explained by a fact specific to stacking faults that a wave with a long wavelength in a direction parallel to the stacking-fault plane can hardly discriminate between the regular and stacking-fault structures. However, the directional dependence and the nearly zero reflection in the most region are not trivial. We explain these properties as follows.

We consider a Schrödinger equation expressed in terms of a localized basis as

$$V_0^\dagger \mathbf{C}_{n-1} + H\mathbf{C}_n + V_0\mathbf{C}_{n+1} = E\mathbf{C}_n, \tag{1}$$

for $n \neq 0, 1$ and

$$V_0^\dagger \mathbf{C}_{-1} + H\mathbf{C}_0 + V\mathbf{C}_1 = E\mathbf{C}_0, \tag{2}$$

and

$$V^\dagger \mathbf{C}_0 + H\mathbf{C}_1 + V_0\mathbf{C}_2 = E\mathbf{C}_1. \tag{3}$$

$\mathbf{C}_n$ is a vector composed of the coefficients of atomic orbitals in the nth layer. H is a Hamiltonian matrix composed of the matrix elements between atomic orbitals within each layer. V_0 is also a Hamiltonian matrix between the n and $n+1$

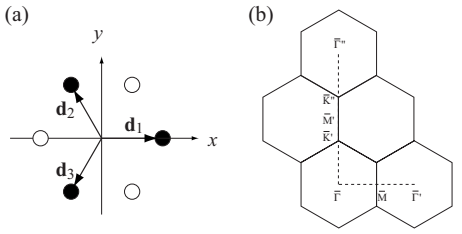

FIG. 3. (a) positions of the nearest neighbor atoms in the neighboring layer projected onto the plane containing the basal atom. Closed and open circles show the atoms in the normal and stacking-fault layers, respectively. (b) labeling of symmetry points in the reciprocal space. The hexagon containing the $\bar{\Gamma}$ point at the center shows the first Brillouin zone.

layers. We assume that a stacking fault is inserted between the 0th and first layers, and therefore the Hamiltonian matrix between these layers is changed to V. A feature of the stacking fault is that the intralayer Hamiltonian matrix are approximately unchanged in the stacking-fault layers. Another feature is that absolute values of the matrix elements in the interlayer Hamiltonian matrix are also approximately unchanged. The character of the stacking fault appears as the difference in phase between the matrix elements of V_0 and V.

First we consider a single-orbital case. It is obvious that when $|V|$ is equal to $|V_0|$, a solution is $C_n = e^{ikan}C_0$ for $n \leq 0$ and $C_n = e^{-i\delta}e^{ikan}C_0$ for $n \geq 1$, where k and a are a wave number and a lattice constant. δ is a phase given by $V/V_0 = e^{i\delta}$. This result means that the reflection probability is zero, and the stacking fault changes only the phase of the transmitted wave. When $|V|$ is not equal to $|V_0|$, transmission probability T is given by

$$T = \frac{1 - \cos(\Delta ka)}{(\alpha^2 + 1/\alpha^2)/2 - \cos(\Delta ka)}, \tag{4}$$

where $\alpha = |V/V_0|$ and $\Delta k = k_+ - k_-$. k_+ and k_- are wave numbers of the waves propagating in positive and negative directions, respectively. Δk is zero on the rim of the constant-energy surface. Therefore the transmission probability is zero when α is not equal to 1.

Here we consider the case of the stacking fault. If the wave function is composed only of a single s wave and we take account only of the nearest-neighbor transfer energy, V_0 is given by

$$V_0 = V_{ss\sigma}(e^{i\mathbf{q}\cdot\mathbf{d}_1} + e^{i\mathbf{q}\cdot\mathbf{d}_2} + e^{i\mathbf{q}\cdot\mathbf{d}_3}), \tag{5}$$

where $\mathbf{q}$ is a two-dimensional wave vector parallel to the stacking-fault plane. $\mathbf{d}_1$, $\mathbf{d}_2$, and $\mathbf{d}_3$ are two-dimensional vectors pointing at the positions of the nearest-neighbor atoms in the neighboring layer projected onto the plane containing a basal atom. Since the projected positions of atoms in the stacking-fault layer have inversion relation to the regular positions as shown in Fig. 3, V in the stacking-fault layer is equal to V_0^*, and the transmission is always perfect. This result holds for non-s-waves and non-nearest-neighbor atoms. Therefore at least two kinds of orbitals are necessary for explaining the strong reflection near the $\bar{M}$ point in Fig. 2.

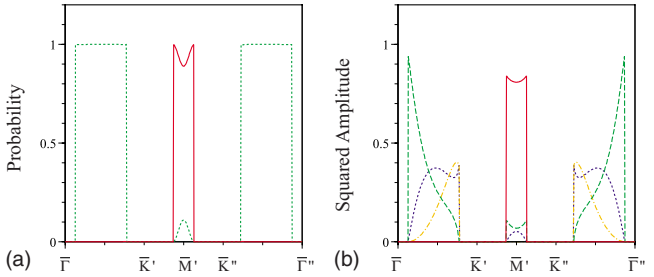

FIG. 4. (Color online) (a) reflection (red solid line) and transmission (green broken line) probabilities on the $\bar{\Gamma}$-$\bar{K}'$-$\bar{M}'$-$\bar{K}''$-$\bar{\Gamma}''$ line shown in Fig. 3(b). (b) Squared amplitude of components in the incident wave on the same line. Solid (red), broken-dotted (orange), broken (green), and dotted (blue) lines show the p_x, p_y, p_z, and s components.

By analogy with the single-orbital case, we obtain the conditions for perfect transmission in the multiorbital case as

$$V\mathbf{D} = e^{i\delta}V_0\mathbf{D}, \tag{6}$$

and

$$V^\dagger\mathbf{D} = e^{-i\delta}V_0^\dagger\mathbf{D}, \tag{7}$$

where $\mathbf{D}$ is an incident wave which is an eigenvector of translation in a periodic system given by Eq. (1). These equations mean that scattering effects are canceled out by renormalization using single phase δ. Actually these conditions are usually too tight to satisfy. However, they can approximately be satisfied in the case of stacking faults due to the geometrical symmetry as follows.

Since d orbitals can be neglected near the Fermi energy of Ag, we consider only the s, p_x, p_y, and p_z orbitals for simplicity. We set the x and y axes as Fig. 3, and the z axis to the direction perpendicular to the xy plane. First we consider the case that two-dimensional wave vector $\mathbf{q}$ is parallel to the y axis. Since the positions of atoms in the normal and stacking-fault layers are symmetrical each other with respect to the y axis, phase factors $e^{-i\mathbf{q}\cdot\mathbf{d}_1}$, $e^{-i\mathbf{q}\cdot\mathbf{d}_2}$, and $e^{-i\mathbf{q}\cdot\mathbf{d}_3}$ in V have the same values as those of the atoms in the symmetrical positions in V_0. Therefore, the matrix elements in V between the orbitals which have the same symmetry with respect to y axis are equal to those in V_0. V and V_0 differ in the matrix elements between orbitals having different parity, namely, between the p_x orbital and the s, p_y, and p_z orbitals. Therefore, if incident wave $\mathbf{D}$ has nonzero components only of the same symmetry, Eqs. (6) and (7) are satisfied, and transmission is perfect.

Figure 4 shows the components of the incident wave as a function of wave vector $\mathbf{q}$ running on the y axis. $\bar{M}'$ and $\bar{\Gamma}''$ are the points in the first-neighbor and second-neighbor Brillouin zones, respectively, as shown in Fig. 3(b). The transmission and reflection probabilities on this line are also shown in the figure. The regions where both the transmission and reflection probabilities are zero have no propagating mode. The correspondence between the orbital components and the transmission property is clear. The transmission is almost perfect in the regions between $\bar{\Gamma}$ and $\bar{K}'$ points where

the asymmetrical p_x component can be neglected and the incident wave consists of the orbitals of the same symmetry. This result can intuitively be understood by knowing that the wave in this form does not feel the difference between the regular and stacking-fault structures. The reflection is strong in the region near the $\bar{M}'$ point where the p_x component is large and mixed with other components of different symmetry.

The reason for the large mixing of the orbitals with different symmetries near $\bar{M}'$ or $\bar{M}$ is as follows. For example, we consider the matrix element between the s and p_x orbitals given by

$$\frac{V_{sp\sigma}}{\sqrt{3}} e^{i\mathbf{q}\cdot\mathbf{d}_1}\left[1 - \frac{e^{i\mathbf{q}\cdot(\mathbf{d}_2-\mathbf{d}_1)} + e^{i\mathbf{q}\cdot(\mathbf{d}_3-\mathbf{d}_1)}}{2}\right]. \tag{8}$$

This matrix element is zero at $\mathbf{q}=0$, and the absolute value is largest at the $\bar{M}$ point due to the constructive interference of the three waves. The matrix element between the p_x and p_z orbitals has similar $\mathbf{q}$ dependence. Therefore the orbitals with different symmetries are mixed in the wave function near the $\bar{M}$ point. On the other hand, the matrix elements between the same kinds of orbitals have a reverse property. The absolute values are large at the $\bar{\Gamma}$ point and decrease with increasing the distance from the $\bar{\Gamma}$ point, as exemplified by the matrix element of the s orbitals shown in Eq. (5). Therefore, a wave consisting of orbitals with different symmetries cannot satisfy the conditions in Eqs. (6) and (7), and is strongly reflected by the stacking fault.

When wave vector $\mathbf{q}$ points to other directions than the y axis, there is no simple explanation for the transmission property. Figure 5 shows the transmission probability and the orbital components of the incident wave on the $\bar{\Gamma}$-$\bar{M}$-$\bar{\Gamma}'$ line, where $\bar{\Gamma}'$ is the point on the x axis in the neighboring Brillouin zone as shown in Fig. 3(b). The reflection is almost zero except for the narrow region including the $\bar{M}$ point. However, the p_x component gradually increases with approaching the $\bar{M}$ point from the $\bar{\Gamma}$ point. The asymmetry in the components with respect to the $\bar{M}$ point is originated from the atomic structures of bulk Ag. Since the fcc lattice has only threefold symmetry with respect to the [111] axis, the neck near the $\bar{M}$ point is directed at a finite angle with the (111) plane in the three-dimensional Fermi surface as shown in Fig. 2(c). When wave vector $\mathbf{q}$ is parallel to the x axis, the wave can recognize the difference in atomic positions between the regular and stacking-fault structures shown in Fig. 3. Therefore it is not clear why the reflection probability is almost zero except for the narrow region.

In order to see how well the condition for the perfect transmission shown in Eq. (6) is satisfied, we calculate a quantity defined by

$$\gamma = \frac{|V\mathbf{D} - e^{i\delta}V_0\mathbf{D}|^2}{|V_0\mathbf{D}|^2}. \tag{9}$$

This normalized difference may be regarded as an index for reflection strength. δ in Eq. (9) is determined from the phase of the transmitted wave. Figure 5 shows the difference and phase. We checked that the difference calculated from the condition shown in Eq. (7) has the same value.

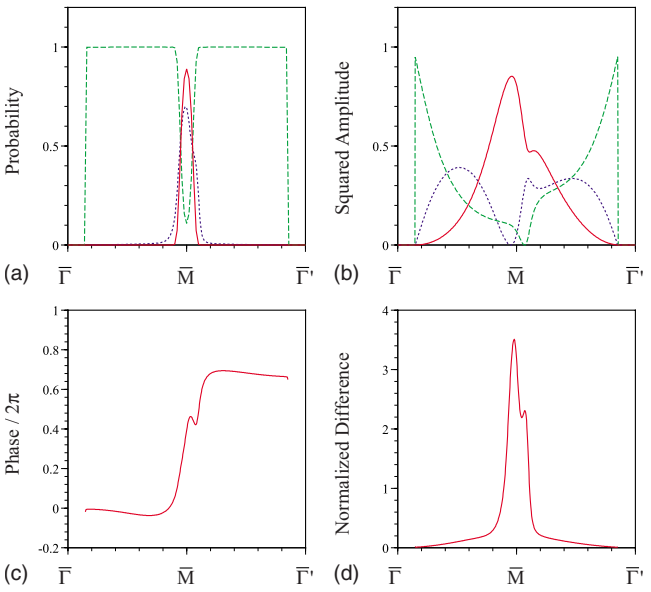

FIG. 5. (Color online) (a) reflection (red solid line) and transmission (green broken line) probabilities on the $\bar{\Gamma}$-$\bar{M}$-$\bar{\Gamma}'$ line shown in Fig. 3(b). Dotted (blue) line shows approximate reflection probability. (b) Squared amplitude of components in the incident wave on the same line. Solid (red), broken (green), and dotted (blue) lines show p_x, p_z, and s components. The p_y component is zero. (c) phase difference δ between the incident and transmitted waves. (d) normalized difference γ defined in Eq. (9). The phase difference in (c) is used for calculating γ.

As expected, the normalized difference is small and large near the $\bar{\Gamma}$ and $\bar{M}$ points, respectively. However, the difference remains small even in the intermediate region of these points, where the p_x component has the same order of amplitude as the p_z and s components. The difference is large only in the narrow region near the $\bar{M}$ point. This behavior is similar to that of the reflection probability.

The phase is not zero but $2/3\times 2\pi$ near the $\bar{\Gamma}'$ point. This reflects the periodicity of the Hamiltonian with respect to the in-plane wave vector. The phase is close to zero in the most region of the first Brillouin zone, and changes largely near the $\bar{M}$ point where the reflection probability is large.

An analysis of the wave function shows that the amplitudes of the evanescent components are negligibly small in the region where the transmission is almost perfect. The evanescent components have large amplitude only near the $\bar{M}$ point. This means that in the nearly perfect transmission the incident wave can pass through the stacking fault without deformation by the aid of evanescent waves.

There is a difference in the behavior between the reflection probability and normalized difference γ. The reflection probability is almost zero in the intermediate region, but γ is not necessarily almost zero. This discrepancy may be explained by the difference in the phase factor between the incident and reflected waves. The transmission probability for the single-orbital case shown in Eq. (4) has factor Δka.

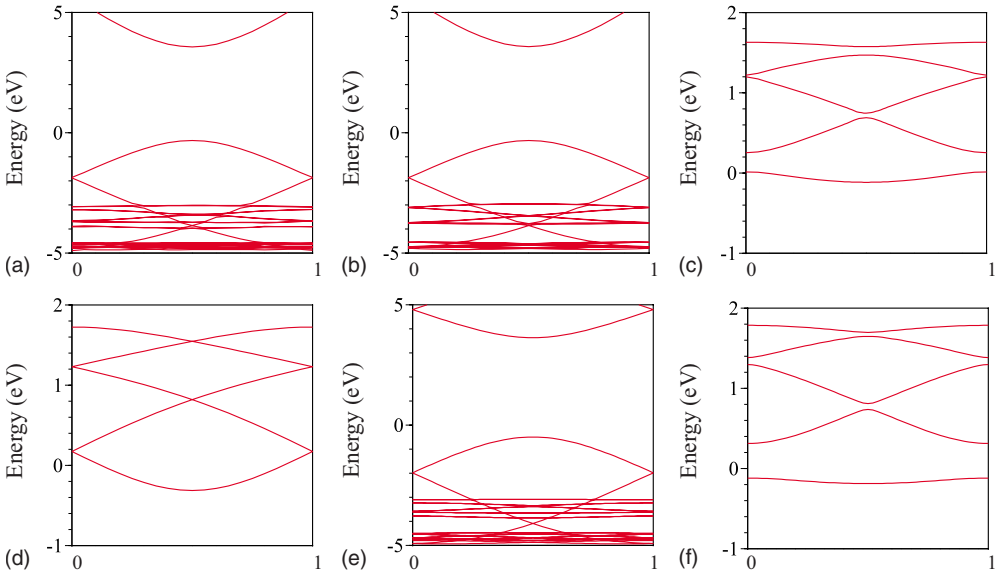

FIG. 6. (Color online) Band structures of a stacking-fault superlattice (a), (c), (e), (f) and a system without stacking faults (b), (d) calculated by a density-functional method (a), (b), (c), (d) and a tight-binding method (e), (f). The parallel components of a wave vector are fixed at the $\bar{\Gamma}$ point (a), (b), (e) and the $\bar{M}$ point (c), (d), (f) in the two-dimensional Brillouin zone. Horizontal axis shows the coefficient of the reciprocal lattice vector perpendicular to the stacking-fault plane.

When this factor is close to π, the transmission probability is large. This means that when the wavelengths of the incident and reflected waves do not match, the incident wave is hard to reflect. We calculate the reflection probability by using Eq. (4) where α is estimated by assuming $\alpha^2 \sim 1+\gamma$. Figure 5(a) shows this approximate reflection probability in comparison with the exact one numerically obtained. Though quantitative agreement may not be enough, the approximate probability explains better the exact one. This result suggests that two factors seem important to explain the anomalous perfect transmission through the stacking fault. One is the nondeformability of the wave form at the stacking fault as expressed in Eqs. (6) and (7). Second is the phase difference between the incident and reflected waves.

2. Three-dimensional superlattices

Before presenting results for thin films, we show the results for three-dimensional stacking-fault superlattices. Figure 6 shows band structures of a stacking-fault superlattice where stacking faults are introduced every five layers in the fcc structure of bulk Ag. The energy bands are calculated with fixing the components of a wave vector parallel to the stacking-fault plane and shown as a function of the perpendicular component. The horizontal axis in the figures shows the coefficient of the primitive vector of the reciprocal lattice perpendicular to the stacking-fault plane. Since the other two primitive vectors are not perpendicular to the stacking-fault plane, the zeros in the horizontal axis do not necessarily mean that the perpendicular component of a wave vector is zero.

As expected from the map of reflection probability shown in Fig. 2, the stacking fault has almost no effect on the states at the $\bar{\Gamma}$ point near the Fermi energy, and opens band gaps in the bands at the $\bar{M}$ point. We checked that the band structures at the $\bar{K}$ point also show almost no difference between the systems with and without stacking faults. The band structures obtained by the tight-binding method reproduce those by the density-functional method with errors of 0.18 eV at maximum. This inaccuracy may originate from the choice of the tight-binding parameters and the neglect of the higher-order neighbor terms in transfer energy.

B. Stacking faults in thin films

We present calculations for the atomic structures shown in Fig. 7. The thin films have (111) surfaces and the stacking-fault plane is, for example, the $(11\bar{1})$ plane. Therefore, the stacking-fault plane is not perpendicular to the surface plane but tilted by an angle given by $\tan^{-1}(1/\sqrt{8})$. The introduction of a stacking fault into a film produces a step on the surface of the film. The height of this step is 1/3 monolayer and steps run in the $[1\bar{1}0]$ direction. The model proposed by Uchihashi *et al.*[3] is the single stacking-fault structure. The double

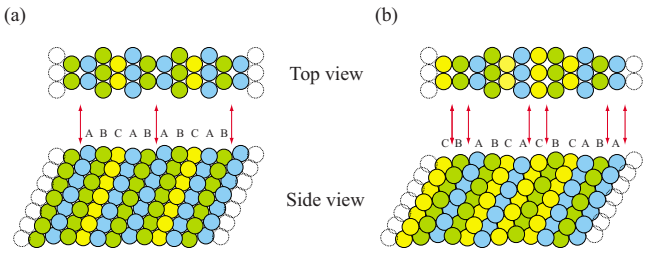

FIG. 7. (Color online) Schematic of atomic structures of the Ag(111) stacking-fault superlattice films. (a) Single stacking-fault and (b) double stacking-fault structures. Red arrows indicate the positions where stacking faults are inserted. A, B, and C show the stacking sequence.

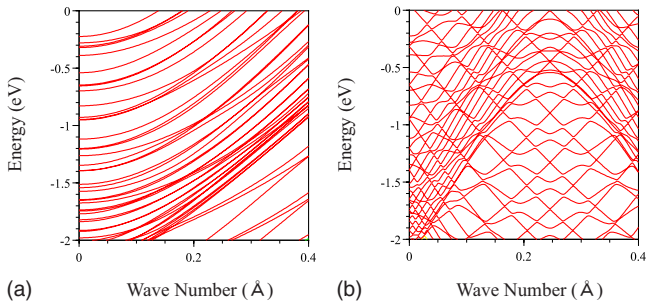

FIG. 8. (Color online) Bands structures of a single stacking-fault film. The wave vector is (a) parallel and (b) perpendicular to the surface step line produced by an introduction of a stacking fault. The thickness of the film is 26 layers.

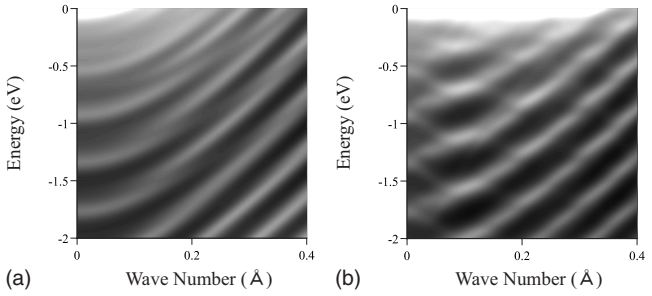

FIG. 9. Energy spectra defined by Eq. (10) calculated for a single stacking-fault film, corresponding to the band structures shown in Fig. 8. The wave vector is (a) parallel and (b) perpendicular to the surface step line of a stacking fault. The thickness of the film is 26 layers.

stacking-fault structure proposed in this paper has subsequent introductions of two stacking faults. The surface unit cells of both structures contain five layers in the direction perpendicular to the step lines. However, the shape of the surface unit cell is rectangular and oblique in the single and double stacking-fault structures, respectively.

The lattice period of the substrate Si(111)4×1-In surface is 13.3 Å in the direction perpendicular to the In chains. The corresponding periods are 12.8 and 13.2 Å for the single and double stacking-fault structures, respectively. Therefore, if we consider only the commensurability with the substrate, the double stacking-fault structure is more favorable in elastic energy than the single one. However, the single one may have the advantage of less formation energy of stacking faults, and the interaction with substrates may be important at the initial stage of growth. The discussion on the atomic structures with taking account of these factors is out of the scope of the present paper. Therefore we present results for both structures.

1. Single stacking-fault structure

Figure 8 shows band structures of a Ag (111) film in the single stacking-fault structure calculated by the tight-binding method. The number of layers is 26 which is the same as that of the sample whose energy dispersion was measured in the photoemission experiment.[8] The energy bands parallel to the surface step line of the stacking fault have free-electron-like dispersions. The band structure in the perpendicular direction is complex due to the band folding. The band structures obtained in the photoemission experiments[8,9] do not show the folded structures of superlattices but 1×1 unfolded structures similar to those of Ag(111) films without stacking faults. Therefore we calculate unfolded bands using a method shown in the following. There are sophisticated methods for calculating the photocurrent spectra in photoelectron spectroscopy.[26] However, we do not calculate the photocurrent spectra but only unfold the folded bands because we do not compare the photocurrent spectra with experiments but only discuss the origin of the formation of the flat band dispersions by comparing the band structures with experiments in this paper.

To compare with the energy dispersions obtained by photoemission, we calculate a spectrum given by

$$\rho(\mathbf{k},E)=\sum_i |M_{l\mathbf{k}}|^2 w(E-E_{l\mathbf{k}}), \tag{10}$$

where $\mathbf{k}$ and E are a two-dimensional wave vector and energy. $E_{l\mathbf{k}}$ is the energy of an electron in the lth band with $\mathbf{k}$. We evaluate matrix element $M_{l\mathbf{k}}$ by

$$M_{l\mathbf{k}}=\sum_{m,n} C_{l\mathbf{k},mn}, \tag{11}$$

where $C_{l\mathbf{k},mn}$ is a coefficient of the mth atomic orbital of the nth atom in a unit cell. Only the atoms in the outermost layer are taken in the summation. This reflects the fact that photoemission spectroscopy is sensitive to surfaces due to the small escape depth of electrons.[26] We choose the Lozentzian function for function $w(E)$. The width of energy is 0.1 eV.

Figure 9 shows spectra calculated for the Ag film with single stacking faults. The states with long wavelengths emerge from the folded bands shown in Fig. 8. The regions with strong intensity near 0 eV are due to contribution of the *sp* surface state.

The bands in the spectra parallel to the step line have free-electron-like dispersions with slight residuals of the folded bands. In contrast the bands perpendicular to the step line are considerably deformed. Though the bands roughly preserve the shape of the parabolic dispersion, they seem segmentalized. This is caused by the coupling with the folded bands as discussed in Sec. III B 3. As a result the bands tend to be flatten. These features agree with the band structures obtained by experiments.[8,9] The experimental bands are flat near the zero in wave number and have discontinuity at about 0.2 $Å^{-1}$. The free-electron-like dispersions are recovered in the outside of the discontinuity.[9]

However, there are several disagreements between the present calculation and the experiments in the details. One is that the bands are flat at the zero wave number in the experiments but not in the calculation. The relatively flat regions are shifted from the band center in the calculation. The second one is that the degree of flatness seems insufficient in the calculation. These observations lead to an idea that the electron confinement may not be sufficient in the atomic structure with single stacking faults. Therefore we propose a structure with double stacking faults shown in Fig. 7(b) as a candidate for the Ag films on the Si(111)4×1-In surface.

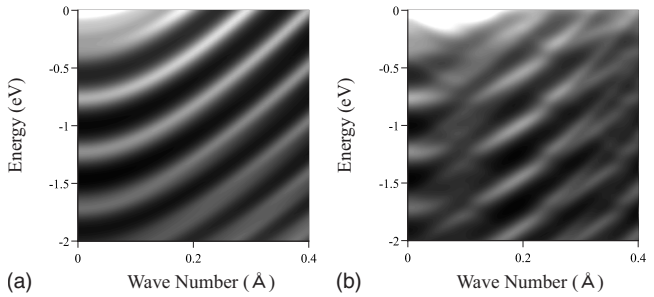

FIG. 10. Energy spectra defined by Eq. (10) calculated for a double stacking-fault film. The wave vector is (a) parallel and (b) perpendicular to the surface step line of a stacking fault. The thickness of the film is 26 layers.

Since this structure has two stacking faults in a unit cell, electron confinement is expected to be stronger than the single stacking-fault structure. Though this structure has a loss in the formation energy of stacking faults, there is an advantage of good commensurability with the substrate. So we calculate the electronic structure of the double stacking-fault structure.

2. Double stacking-fault structure

Figure 10 shows energy spectra defined in Eq. (10) calculated for the double stacking-fault structure shown in Fig. 7(b). The thickness of the Ag film is 26 layers. The bands parallel to the step line have free-electron-like dispersions, and the perpendicular ones are considerably deformed, which is the same as the single stacking-fault structure. However, the degree of deformation in the perpendicular bands is larger than the single stacking-fault one as expected. In addition, the bands are flat at the zero wave number, which agrees with the experimental bands.[8,9] These results suggest a possibility that the Ag films on the Si(111)4×1-In surface are in the double stacking-fault structure. It is a matter of course that the atomic structure of the Ag films cannot be determined only from the present calculation.

There is a quantitative difference in the energy positions of the quantized bands between the calculation and experiment. The binding energies at the zero wave number are about 0.3, 0.6, 0.9, 1.4, and 1.8 eV in the experiment.[8] The calculated ones are 0.4, 0.8, 1.2, 1.7, and 2.2 eV. One reason for this discrepancy may be inaccuracy of the tight-binding parameters. The present tight-binding parameters reproduce the band structures of the density-functional calculations with errors of about 0.1 eV. The discrepancy may be originated also from the neglect of the substrate in the present calculation. The phase of reflection at an interface of a Ag film and a substrate depends on the condition of continuity of a wave function at the interface, and can be different from that of a free-standing Ag film in principle. The systematic difference in the spacing of quantized energy levels suggests a possibility that the effective thickness of the Ag film on the substrate in the experiment may be larger than 26 layers due to the phase shift at the interface.

Here we discuss the mechanism of the strong deformation in the band structures based on the transmission property through the bulk stacking fault shown in Sec. III A 1. As shown in Fig. 2, reflection is strong near the rim of the constant-energy surface on the $\bar{\Gamma}$-$\bar{M}$ line. We denote the wave number at the rim on this line by q_c, where q_c is a function of energy E. Since the stacking fault is inserted into the position of the thin films shown in Fig. 7, the surface normal vector projected onto the stacking-fault plane is aligned with the $\bar{\Gamma}$-$\bar{M}$ line. The waves constituting the bottom state of each quantized subband in thin films have wave vectors normal to the surface. Therefore, if the stacking-fault plane were perpendicular to the surface, the wave number of the bottom state corresponds to the rim on the $\bar{\Gamma}$-$\bar{M}$ line, where reflection is strong.

Actually there are mainly two factors in deviation of the wave number from q_c. One is the tilt of the stacking-fault plane with respect to the surface normal. Since the tangent of the tilt is $1/\sqrt{8}$ in the present system, the wave number of the bottom state is multiplied by a factor of $\sqrt{8}/3=0.94$. The deviation by 6% from q_c is not large. The tilt of the stacking-fault plane produces a qualitative effect on the band structures in a different way as shown in the next subsection. Second is the finiteness of spacing between the stacking-fault planes. When the confinement by stacking faults is strong, the minimum wave number parallel to the surface is not zero but π/L where L is the spacing of stacking faults. Since the wave number at the $\bar{M}$ point is $2\pi/(\sqrt{3}d)$ where d is the distance between Ag atoms, the wave number of the bottom state is multiplied by a factor of $[1-(\sqrt{3}d/2L)^2]^{1/2}$. Since d and L are 2.89 and 13.3 Å, the factor is 0.98. The deviation of 2% is also small. Therefore it may be concluded that the fact that the stacking-fault thin films have the (111) surface is the origin of the strong reflection at stacking faults, which forms the one-dimensional quantized band structures observed in the photoemission experiments. This result leads to a following conjecture. If there are thin films which contain stacking faults periodically and have surfaces normal to the $\bar{\Gamma}$-$\bar{K}$ direction such as the (110) surface, the electrons would not be confined by stacking faults and the band structures would also remain similar to that of a free electron.

3. Kronig-Penney model: tilting effect of stacking-fault planes

As shown in Fig. 7, the stacking-fault plane in the present system is not perpendicular to the surface plane but tilted. We discuss the tilting effect on band structures using a simple model. We consider a two-dimensional system which is infinite in x direction and has finite length L_y in y direction. We assume that the potential in a Schrödinger equation is given by

$$V(x,y)=\sum_n v_0 a\,\delta(x-na-\alpha y), \tag{12}$$

where a is the spacing of potential barriers. α and v_0 express the tilt and strength of the barriers.

When the barriers are absent, the wave function is given by

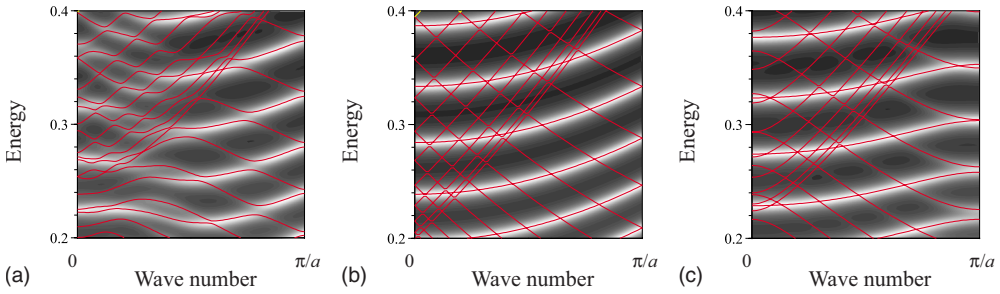

FIG. 11. (Color online) Band structures (red lines) and energy spectra (grayscale maps) of a two-dimensional Kronig-Penney model. Potential strength v_0 is (a), (c) 0.03 and (b) 0. Titling parameter α is (a) $1/\sqrt{8}$ and (c) 0.

$$\phi_{k,n}(x,y) = \frac{1}{\sqrt{L_x}} e^{ikx} \sqrt{\frac{2}{L_y}} \sin\left(\frac{n\pi}{L_y} y\right), \tag{13}$$

where L_x is the length introduced for imposing a periodic boundary condition on the x direction. n is an integer expressing the indices of subbands.

When the barriers are present, the matrix element between two states is calculated as

$$\langle \phi_{k',m} | V | \phi_{k,n} \rangle = \delta_{k,k'+G} 2v_0 \int_0^1 e^{ipy} \sin(m\pi y) \sin(n\pi y) dy, \tag{14}$$

where p is given by $p=\alpha G_x L_y$, and G_x is a reciprocal vector in the x direction. p is a parameter which determines the strength of mixing between states in different subbands.

When the barriers are not tilted, the states in different subbands are decoupled. The periodic potential opens gaps at the center and boundaries of a Brillouin zone. Since the state at the bottom of a subband has no degenerate state in the same subband, the periodic potential causes only a constant shift of the band near the bottom in the first-order perturbation.

When the barriers are tilted, the states in different subbands can be coupled. The states at the bottoms of subbands with relatively high index n may have nearly degenerated states in different subbands, and they can strongly mix. In this case the potential scattering causes a considerable change in band dispersions.

The absolute value of the integral in Eq. (14) is large when the absolute value of p is around $|m-n|\pi$ or $(m+n)\pi$. The geometric meaning of this condition is that the difference between wave vectors of an incident wave and a scattered wave is perpendicular to the barrier line. This is equivalent to the momentum conservation parallel to the barrier line, which is perfect in the limit of infinite L_y.

In order to demonstrate the things mentioned above we calculate the energy bands of the Kronig-Penney model by expanding the wave function in plane waves. We solve a dimensionless Schrödinger equation with $m=1$ and $\hbar=1$ in this subsection. Figure 11 shows energy bands and spectra. a and L_y are 10 and 50, respectively. v_0 is 0.03. α is $1/\sqrt{8}$ which is the same value as the tilt of the stacking-fault plane in the Ag films. The spectra are calculated with a weight of the components with $G_x=0$ in the wave function. Energy levels are broadened by a Lorentzian function with 0.005 in energy width. If we regard a and L_y as 10 and 50 Å which are approximate lengths of the Ag films with about 20 layers, the units of energy are 0.28 hartree. Therefore 0.1 energy in the dimensionless units corresponds to 0.76 eV, and the energy scale is comparable with the bands and spectra shown in Figs. 8–10. Here we assume that the effective mass of Ag bulk bands is the same as the electron mass in vacuum. For comparison, the bands with no barrier ($v_0=0$) and with no tilt ($\alpha=0$) are also shown in the figure.

It is clear that the tilt of barriers causes the mixing of nearly degenerated states in different subbands, and the bands near the bottoms of subbands are considerably deformed. In particular, the bands with positive curvatures are turned to those with negative ones. The bottom bands in the nontilted system undergo only constant shifts and a slight increase of the effective mass by a factor of 1.2 in the present parameters.

Figure 12 shows the wave function of the state with energy $E=0.225$ and wave number $k=0$ shown in Fig. 11(a). The squared amplitude of the wave function is shown in the figure. The wave function is well confined in the regions separated by the barriers. The main component of the wave function is the state at the bottom of the subband with $n=11$. The fraction of the components with $G_x=0$ is 0.85. Most components of the rest are the states with $G_x=\pm 2\pi/a$ with $n=7$, 4, and 8 in the order of magnitude. Since p is 3.54π in the present case, it is natural that the components with $n=7$ and 8 is large. The reason for the

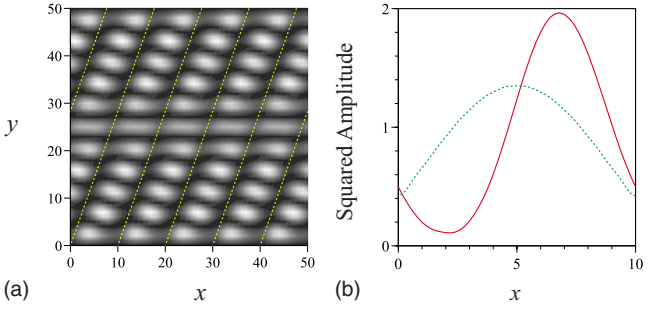

FIG. 12. (Color online) (a) Wave function at energy $E=0.225$ and wave number $k=0$ in Fig. 11(a). The squared amplitude of the wave function is shown. Dotted lines show the positions of barriers. (b) Squared amplitude of the wave function on line $y=7$ shown in (a). Dotted line shows the squared amplitude of the wave function without tilt on the same line.

relatively large mixing of the state with $n=4$ is that the energy of this state is close to that of the main component with $n=11$.

The fraction of the component with $G_x=0$ can be used for an index expressing the strength of confinement. The value of this fraction is one in the absence of potential barriers, and decreases monotonically with increasing the confinement strength. The fraction for the state at the bottom of the subband with $n=11$ is 0.97 in the nontilted system. The difference in fraction between the titled and nontilted cases indicates that confinement is strengthen by titling. The wave functions on line $y=7$ shown in Fig. 12(b) actually demonstrate stronger localization in the tilted system. We checked that this difference does not originated from the elongation of the barrier length by tilt. Note that the fraction of the component with $G_x=0$ is $8/\pi^2(=0.81)$ for the perfect confinement in the one-dimensional Kronig-Penney model, which is calculated from the wave function confined in a quantum well by infinite barriers. Therefore the confinement is fairly strong in the tilted case. The confinement of the Ag thin films by stacking faults is assisted by the tilt of the stacking-fault planes.

IV. CONCLUSION

We have presented a theoretical study on the electronic states of the Ag thin films which contain stacking faults periodically in a direction parallel to the surface. The electronic states of the Ag films are expressed in terms of a tight-binding method. The tight-binding parameters are determined by fitting the band structures to the results calculated by a density-functional method.

We have calculated the band structures of the single and double stacking-fault models. The former was originally proposed for the Ag thin films grown on the Si(111)4×1-In surface, and the latter is proposed in this paper as a structure having less lattice mismatch. The calculated results showed that the double stacking-fault model better reproduces the band structures obtained in the photoemission experiments. It is obvious that only the present result is not enough, and more experimental and theoretical studied are necessary for determining the structures of the Ag films on the Si(111)4×1-In surface.

We have discussed the origin of the strong deformation in the band structures of the stacking-fault thin films based on the transmission property through the bulk stacking fault. The region where the reflection at the stacking fault is strong is limited only near the rims of the three-dimensional constant-energy surface on the $\bar{\Gamma}$-$\bar{M}$ line. The strong deformation is originated from the fact that the stacking-fault thin films have the (111) surface, and the wave vectors of the bottom states in the quantized subbands point near the rim on this line. This result suggests that the deformation in band structures depends on the surface direction of thin films and it may be absent in such thin films having the (110) surface.

Since the stacking-fault planes in the Ag thin films are titled with respect to the direction normal to the surfaces of the thin films, we have studied the tilting effect using a two-dimensional Kronnig-Penney model. The tilt of stacking-fault planes induces the mixing among states in different subbands which are decoupled without tilts. This mixing brings about new effects on the band structures of thin films in addition to the usual effects of the simple non-titled periodic potential. In particular the states near the bottom of each quantized subband, which do not couple with other states without tilts, couple with states in different subbands. This causes drastic changes in the band structure near the bottom of the subband, and bands having even negative effective mass appear in the case of strong mixing. Since the bands near the bottoms of quantized subbands are observed in the photoemission experiments, the titling is an important factor for explaining the observed flat dispersions in addition to the confinement effect intrinsic to stacking faults.

We have discussed the mechanism of the anomalous perfect transmission through the bulk stacking faults. A characteristic feature of stacking faults is that in contract to the usual potential scattering, stacking faults change only the phase of orbitals. The symmetry in atomic positions between the regular and stacking-faults structures with respect to an axis on the stacking-fault plane provides no difference to discriminate these structures for the waves traveling parallel to this axis on the plane. This special symmetry of stacking faults is the origin of the absence of reflection in this direction and causes the directional dependence in the transmission property. The general condition for perfect transmission through stacking faults is that the effects of scattering are canceled out by renormalization using single phase factor. The excellent satisfaction of this condition gives rise to the anomalous perfect transmission through the stacking faults in noble metals.

In this paper we have studied the electronic properties of stacking faults that are periodically inserted into low-dimensional materials on nanometer scales. In this respect it is interesting to study the electronic states of the twinning superlattice nanowires which were recently synthesized.[27,28]

ACKNOWLEDGMENTS

We thank the members of the Frontier Simulation Software for Industrial Science Project for enabling us to use the program package PHASE. We thank Taichi Okuda and Iwao Matsuda for useful comments and discussions. Numerical calculations were performed by using supercomputers at the Institute of Solid State Physics, The University of Tokyo. T.U. thanks JSPS for the financial support KAKENHI Grant No. 21510110.

[1] *The Physics of Metals 2 Defects*, edited by P. B. Hirsch (Cambridge University Press, Cambridge, England, 1975).
[2] D. Hull and D. J. Bacon, *Introduction to Dislocations* (Butterworth-Heinemann, Oxford, 2001).
[3] T. Uchihashi, C. Ohbuchi, S. Tsukamoto, and T. Nakayama, Phys. Rev. Lett. **96**, 136104 (2006).
[4] O. Bunk, G. Falkenberg, J. H. Zeysing, L. Lottermoser, R. L. Johnson, M. Nielsen, F. Berg-Rasmussen, J. Baker, and R. Feidenhans'l, Phys. Rev. B **59**, 12228 (1999).
[5] H. R. Miwa and G. P. Srivastava, Surf. Sci. **473**, 123 (2001).
[6] J. Nakamura, S. Watanabe, and M. Aono, Phys. Rev. B **63**, 193307 (2001).
[7] J. H. Cho, D.-H. Oh, K. S. Kim, and L. Kleinman, Phys. Rev. B **64**, 235302 (2001).
[8] N. Nagamura, I. Matsuda, N. Miyata, T. Hirahara, S. Hasegawa, and T. Uchihashi, Phys. Rev. Lett. **96**, 256801 (2006).
[9] T. Okuda, Y. Takeichi, K. He, A. Harasawa, A. Kakizaki, and I. Matsuda, Phys. Rev. B **80**, 113409 (2009).
[10] H. Bross, J. Phys. F: Met. Phys. **12**, 2883 (1982).
[11] M. D. Stiles and D. R. Hamann, Phys. Rev. B **38**, 2021 (1988).
[12] M. D. Stiles and D. R. Hamann, Phys. Rev. B **41**, 5280 (1990).
[13] M. Murayama and T. Nakayama, J. Phys. Soc. Jpn. **61**, 2419 (1992).
[14] M. Murayama and T. Nakayama, Phys. Rev. B **49**, 4710 (1994).
[15] Z. Ikonić, G. P. Srivastava, and J. C. Inkson, Solid State Commun. **86**, 799 (1993).
[16] Z. Ikonić, G. P. Srivastava, and J. C. Inkson, Phys. Rev. B **48**, 17181 (1993).
[17] K. Kobayashi, Phys. Rev. B **53**, 11091 (1996).
[18] PHASE is a free computer software for band calculations based on first-principles pseudopotential method which is a result from the Frontier Simulation Software for Industrial Science Project. Version 7.01 is used.
[19] D. Vanderbilt, Phys. Rev. B **41**, 7892 (1990).
[20] J. P. Perdew, K. Burke, and M. Ernzerhof, Phys. Rev. Lett. **77**, 3865 (1996).
[21] P. T. Coleridge and I. M. Templeton, Phys. Rev. B **25**, 7818 (1982).
[22] F. Reinert, G. Nicolay, S. Schmidt, D. Ehm, and S. Hüfner, Phys. Rev. B **63**, 115415 (2001).
[23] S. LaShell, B. A. McDougall, and E. Jensen, Phys. Rev. Lett. **77**, 3419 (1996).
[24] D. A. Papaconstantopoulos, *Handbook of the Band Structure of Elemental Solids* (Plenum Press, New York, 1986).
[25] K. Kobayashi, Surf. Sci. **583**, 16 (2005).
[26] S. Hüfner, *Photoelectron Spectroscopy: Principles and Applications* (Springer-Verlag, Berlin, 2003).
[27] R. E. Algra, M. A. Verheijen, M. T. Borgström, L. Feiner, G. Immink, W. J. P. van Enckevort, E. Vlieg, and E. P. A. M. Bakkers, Nature (London) **456**, 369 (2008).
[28] P. Caroff, K. A. Dick, J. Johansson, M. E. Messing, K. Deppert, and L. Samuelson, Nat. Nanotechnol. **4**, 50 (2009).